Geometry of Main Chain Motions in Poly(ethyl methacrylate) Monitored by 3D Difference Correlated NMR

S. C. Kuebler, A. Heuer, and H. W. Spiess*

Max-Planck-Institut für Polymerforschung, Postfach 3148, 55021 Mainz, Germany

Received June 25, 1996[⊗]

ABSTRACT: A systematic analysis of the rotational dynamics in poly(ethyl methacrylate) (PEMA) slightly above the glass transition temperature is performed with advanced multidimensional NMR spectroscopy focusing on a 3D difference correlated exchange experiment. This novel technique is capable of obtaining the detailed geometry of motion as well as the time scale of reorientation without employing a specific model. In PEMA, the coupling of the α- and β-process manifests itself in rotational dynamics that comprise both pronounced small angle fluctuations and large angle reorientations. The time evolution of the latter is characterized quantitatively by a dynamic order parameter, $\langle P_2(t)\rangle$, a transient quantity which monitors the randomization of segmental orientation. The molecular orientations are found to remain correlated on a time scale exceeding the mean correlation time of rotational motion as obtained by 2D exchange NMR. A comparison with the results for polystyrene obtained previously indicates smaller effective jump angles and higher geometric restrictions in PEMA. Moreover, the fraction of segments performing large angle displacements is only slowly increasing with time, demonstrating that some segments stay trapped in their environment.

I. Introduction

The α-relaxation in amorphous polymers is intimately linked to structural relaxation of the polymeric backbone. Notable changes of macroscopic properties such as the specific heat, thermal expansion coefficient, and viscosity can be related to a characteristic slowing down and restrictions of molecular dynamics when approaching the glass transition temperature (T_g) from the isotropic melt.[1,2] Several processes with different correlation times are relevant for the dynamics above the glass transition, yielding a nonexponential decay of correlation functions. The high apparent activation energies close to T_g and the non-Arrhenius temperature dependence of correlation times can be often described by the Williams−Landel−Ferry (WLF) equation. Among the experimental techniques suitable to pursue the complex dynamics of structural relaxation,[3] such as fluorescence anisotropy decay,[4] dielectric spectroscopy,[1,5] or photon correlation spectroscopy,[6,7] multidimensional solid state NMR has given extremely valuable contributions.[8] Especially in the vicinity of T_g, advanced multidimensional NMR techniques have elucidated many features of the α-relaxation since the geometry of motion is accessible directly.[9] Examples of the investigation of amorphous polymers include polystyrene (PS),[10,11] atactic polypropylene,[12] polyisoprene,[13] and poly(vinyl acetate).[14]

However, due to the complexity of the collective dynamics, the analysis of 2D NMR spectra generally relies on a motional model. In earlier work, isotropic rotational diffusion with a distribution of correlation times of several decades has been a successful description.[10] However, spectral shapes are rather similar for various physical models and differ only in detail. For instance, later it was demonstrated that spectra of PS could also be fitted equally well by a combination of rotational diffusion and random jumps, indicating that both small and large angle motions are an essential feature of polymer dynamics. The latter model was corroborated by a 3D exchange experiment.[15] Unfortunately, since the measuring time of a 3D spectrum may be on the order of days, it is often not feasible to perform a systematic analysis of the dynamic evolution with time as is done in 2D NMR.

Recently, a comprehensive analysis of the β-relaxation in poly(methyl methacrylate) and poly(ethyl methacrylate) (PEMA) has been performed.[16,17] Molecular motions were elucidated to comprise 180° flips of the carboxyl unit of the side group coupled to a main chain rearrangement, the latter characterized as a restricted rotation around the local chain axis. This coupling is particularly pronounced in PEMA, where the dynamics of the β-process remains anisotropic even above T_g over a considerable temperature range.[18] Photon correlation studies at high pressure were able to resolve the α- and β-processes.[7,19] The influence of the side group of the main chain dynamics was also probed by 2D magic angle spinning (MAS) exchange NMR for higher *n*-alkyl methacrylate polymers.[20]

In this paper, we report the application of a new multidimensional NMR technique to the α-relaxation of PEMA. The experiment combines the high information content of the 3D spectrum with the advantages of a 2D experiment, such as substantially shorter measuring time requirements and analogous data processing.[21] The reorientation of a molecular site is analyzed in terms of a dynamic order parameter, $\langle P_2(t)\rangle$, which is a measure of the loss of correlation of segmental orientation with time, a vanishing order parameter accounting for equilibration of positions. Thus, motional anisotropies may be detected in a straightforward manner. As a first example, this technique has been applied to polystyrene as a typical amorphous polymer. In this investigation, the existence of small angle fluctuations and large angle displacements was confirmed, and both contributions were evaluated in terms of $\langle P_2(t)\rangle$. Since anisotropic chain motions of methacrylates were concluded from ^{13}C-NMR,[16−18] it is interesting to probe the dynamic order parameter for this class of polymers by 3D difference correlated NMR in order to investigate whether this quantity provides a new aspect to compare the difference in the dynamics of various polymers.

Emphasis will be put on a detailed investigation of the motional geometry in PEMA and its comparison to

[⊗] Abstract published in *Advance ACS Abstracts,* September 15, 1996.

S0024-9297(96)00911-4 CCC: $12.00

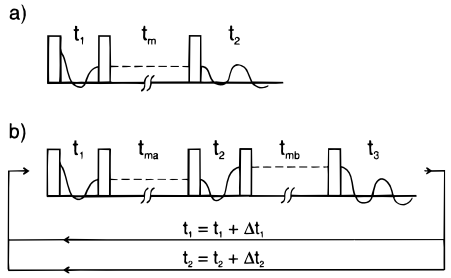

Figure 1. Pulse sequences used in multidimensional exchange NMR: (a) two-dimensional exchange experiment. The evolution time (t_1) is incremented to obtain a 2D data set. Reorientations may take place during the mixing time (t_m). (b) reduced three-dimensional experiment (DICO). Simultaneous incrementation of t_1 and t_2 leads to a data set correlated by difference frequencies (ω_1 and ω_2). The dynamic evolution of segments, which were mobile during the first mixing time (t_{ma}), is analyzed during t_{mb}.

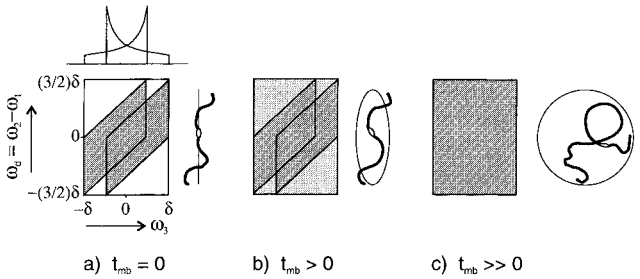

Figure 2. Dynamic evolution of the orientation of a polymer segment with t_{mb} and corresponding DICO spectra as described in the text. The second transition of the ^{2}H nucleus is also incorporated in the contour representation. (a) $t_{mb} = 0$: the exchange intensity caused by reorientations during t_{ma} is confined to the shaded area. (b) reorientation during t_{mb} results in an intensity distribution along the ω_3-axis, indicated by the lighter shading. (c) a complete distribution of orientations leads to symmetric spectra with respect to the slice along $\omega_d = 0$.

PS. A general analysis of the α-relaxation in polymethacrylates below and above the glass transition will be published elsewhere.[22]

II. Background

(a) NMR Spectroscopy. In this section, a short description of the necessary aspects of multidimensional exchange NMR in the solid state is provided. A comprehensive treatment can be found in the literature.[8] Solid-state ^{2}H NMR exploits the anisotropy of the quadrupolar interaction with the angular dependence of the NMR frequency of a molecular site relative to the external magnetic field, B_0, given by

$$\omega_{\pm} = \omega_0 \pm {}^1/_2\delta(3\cos^2\beta) \qquad (1)$$

for an axially symmetric field gradient (**EFG**) tensor, which is a good approximation for aliphatic C−^{2}H sites. Then the unique axis of the **EFG** tensor can be taken along the C−^{2}H bond, reflecting directly its orientation with respect to B_0 by the angle β. ω_0 denotes the Larmor frequency, and the anisotropy parameter is $\delta = (3e^2qQ/4\hbar)$, with the quadrupole coupling constant equaling $e^2qQ/\hbar$. Thus orientations and reorientations of a specific molecular site can be monitored in a straightforward manner. Detailed geometric information about molecular motions on a time scale of a millisecond to seconds can be readily obtained from 2D exchange spectra. Reorientations occurring during a mixing time (t_m) are probed by encoding the angular dependent NMR frequencies during an evolution time (t_1) and reading out the new frequencies during the detection period (t_2) with t_1, $t_2 \ll t_m$ (Figure 1a).

In the slow motion limit, no frequency changes during the evolution and detection period are present. Then the spectrum resulting from incrementation of the evolution time t_1 and double Fourier transform represents the probability of finding a molecule at $\tilde{\omega}_2$ given it had the frequency $\tilde{\omega}_1$ before, when the frequency of a specific nuclear spin is denoted by $\tilde{\omega}$ for a distinction from the frequency axis ω_1 and ω_2 of the spectrum. By varying t_m, the dynamics can be followed in real time. In ^{2}H-NMR, generally off-resonance measurements are not feasible. Instead, fully absorptive 2D spectra are recorded by appropriate combination of the two frequency modulated data sets,[23,24]

$$F_{cc} = \langle \cos\tilde{\omega}_1 t_1 \cos\tilde{\omega}_2 t_2 \rangle \qquad (2)$$

$$F_{ss} = \langle \sin\tilde{\omega}_1 t_1 \sin\tilde{\omega}_2 t_2 \rangle \qquad (3)$$

where $\langle\ \rangle$ denotes the powder average. In absence of motion, the spectrum is confined to the diagonal, i.e. $\tilde{\omega}_1 = \tilde{\omega}_2$. For a broad distribution of reorientation angles, typical for amorphous materials, no characteristic elliptical exchange ridges are observed.[9] Instead, small angle fluctuations manifest themselves in a broadening of the diagonal spectrum, while large angle motions cause featureless exchange intensity spread over large parts of the frequency plane. The 2D experiment can be extended to three dimensions by introducing an additional evolution and mixing time. By this means the dynamic process may be probed twice, providing useful information about the trajectory of a molecular segment. However, since both evolution times have to be incremented independently, measuring time requirements may be quite high. Moreover, in ^{2}H NMR, one has to combine four different data sets to get purely absorptive and undistorted spectra.[24] Some examples exploiting the information content of 3D spectra are discussed in the literature.[8,15]

It is therefore of interest to retain significant information from the 3D spectra while gaining the advantages of a 2D experiment. To this end, a reduced 3D experiment has been developed as outlined in ref 21. Its essential experimental feature is the simultaneous incrementation of both evolution times t_1 and t_2, hence $t_{12} \equiv t_1 = t_2$; see Figure 1b. By adding and subtracting two of the four 3D data sets, respectively, and applying trigonometric relations, one gets

$$F_{cos} = \langle \cos(\tilde{\omega}_1 - \tilde{\omega}_2)t_{12} \cos\tilde{\omega}_3 t_3 \rangle \qquad (4)$$

$$F_{sin} = \langle \sin(\tilde{\omega}_1 - \tilde{\omega}_2)t_{12} \sin\tilde{\omega}_3 t_3 \rangle \qquad (5)$$

Equations 4 and 5 are completely analogous to eqs 2 and 3, and identical data processing can be performed. In the reduced 3D spectrum, the indirect dimension is substituted by the difference frequency, $\omega_d = \omega_2 - \omega_1$, and related to a third frequency, ω_3, as the direct dimension. Therefore, the experiment is denoted 3D *di*fference *co*rrelated spectroscopy (DICO). In comparison to a 3D spectrum, the DICO spectrum represents a projection of the signal intensity of the 3D cube onto the diagonal plane spanned by $\omega_1 = -\omega_2$ and ω_3.

To get a qualitative understanding of the information content of the DICO spectra, their dependence on the two mixing times t_{ma} and t_{mb} will be discussed first as illustrated in Figure 2. The second transition of the ^{2}H

nucleus is also included in the corresponding contour plots. For reorientations taking place during t_{ma} in the limit $t_{mb} = 0$, $\tilde{\omega}_1$ may differ from $\tilde{\omega}_2$ while $\tilde{\omega}_2 = \tilde{\omega}_3$. Accordingly, spectral intensity is found in an interval between 0 and $3/2\delta$ along the ω_d-axis, since the maximum possible frequency change is from $-\delta/2$ to δ. The condition $\omega_2 = \omega_3$ sets the second limit to the accessible frequency range. Therefore, the exchange intensity is confined to the shaded parallelogram in the contour representation (Figure 2a). For finite t_{mb}, reorientations may also occur during the second mixing time, and thus $\omega_2 \neq \omega_3$. Intensity is then distributed along the ω_3-axis, as indicated by the lighter shading of those regions (Figure 2b). A complete exchange of orientations results in a symmetric spectrum with respect to the slice along $\omega_d = 0$; see Figure 2c. Stated differently, when the orientations after the second mixing time are equilibrated, the DICO spectrum $g(\omega_d,\omega_3)$ becomes symmetric, expressed as $g(\omega_d,\omega_3) = g(-\omega_d,\omega_3)$.[21] Components rigid during t_{ma} appear on the slice along $\omega_d = 0$. Then $g(\omega_d{=}0,\omega_3)$ is analogous to the diagonal of the 2D spectrum, irrespective of whether a reorientation during t_{mb} takes place or not. This is easily rationalized by eqs 4 and 5: for $\tilde{\omega}_1 = \tilde{\omega}_2$, the data set $F_{cos} = \langle \cos \tilde{\omega}_3 t_3 \rangle$ is equivalent to its one-dimensional counterpart, while the sine component vanishes. Thus, only the dynamic evolution of molecular sites mobile during t_{ma} can be monitored.

(b) Information Content of DICO Spectra. The goal of the analysis of DICO spectra is to relate the time dependent orientational correlation with respect to the initial state via a simple quantitative measure, such as is provided by a symmetry analysis. In the limit of long mixing times, correlations are completely lost, and for amorphous polymers the reorientation angle distribution (RAD) is isotropic, formulated as $R(\beta) = \sin \beta$. Weak uniaxial anisotropies are commonly described by expanding the NMR spectrum into Legendre polynomials.[8,25] By restricting the sum to the second Legendre polynomial $\langle P_2(\cos \beta) \rangle = \langle \omega/\delta \rangle$, the common "order parameter", and assuming isotropic reorientation during the first mixing time, the frequency distribution of the 3D spectrum is written as

$$p(\omega_1,\omega_2,\omega_3) = p_0(\omega_1)\, p_0(\omega_2)\, p_0(\omega_3)\left[1 + 5\langle P_2 \rangle \left(\frac{\omega_2}{\delta}\right)\left(\frac{\omega_3}{\delta}\right)\right] \tag{6}$$

with $p_0(\omega_i)$ being the powder spectrum. As mentioned above, an isotropic RAD after t_{mb} results in spectral symmetry with respect to the slice along $\omega_d = 0$. Therefore, the degree of anisotropy expressed by $\langle P_2(t) \rangle$ is monitored by the asymmetry of the DICO spectrum. It is important to note that $\langle P_2(t) \rangle$ is not a static property describing the degree of order in a sample, for example, of a nematic liquid crystal, but a transient quantity, changing with time. Thus, $\langle P_2(t) \rangle$ is a probe for the time dependent correlation of a segment at a time t_{mb} with respect to its initial orientation. Specifically the ratio

$$G(x,t) \equiv \frac{g(\omega_d,\omega_3{=}-\delta/2)}{g(-\omega_d,\omega_3{=}-\delta/2)} \tag{7}$$

with the normalized frequency units $x = \omega_d/\delta$ is considered. Figure 3 shows a semilogarithmic plot of $G(x,t)$ versus x for different values of $\langle P_2(t) \rangle$. It clearly reflects the decrease of the order parameter with the ratio $G(x,t)$ approaching 1 for fixed x. The curves suggest a nearly linear relationship between $\langle P_2(t) \rangle$ and $G(x,t)$, which can

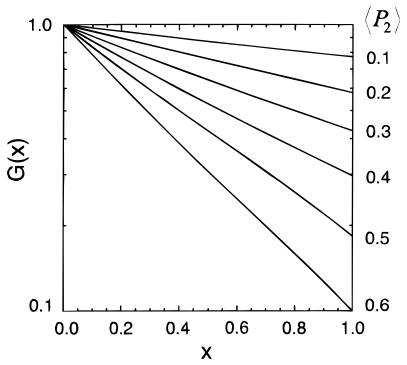

Figure 3. A plot of $G(x,t)$ versus $x = \omega_d/\delta$ for a single type of motion shows a nearly linear relationship between the logarithmic slope of $G(x,t)$ and different dynamic order parameters $\langle P_2(t) \rangle$.

in fact be approximated by

$$\langle P_2(t) \rangle = y - 0.4y^2 \tag{8}$$

with y defined as the logarithmic slope $y \equiv \log(G(0,t)/G(x,t))/x$. A detailed discussion together with the full expression for $G(x,t)$ obtained by evaluation of eq 6 for the DICO spectra is given in ref 21.

Above, it was assumed that a single type of motion is present. The analysis can be extended to two types of motion, distinguished by different dynamic order parameters. For instance, when small angle fluctuations and large angle displacements are present, the reorientation angle distribution decomposes to

$$R(\beta,t) = [1 - f_{jump}(t)]\, R_{fluc}(\beta,t) + f_{jump}(t)\, R_{jump}(\beta,t) \tag{9}$$

There, $f_{jump}(t)$ is the fraction of segments performing large angle (jump-type) motions associated with conformational transitions (see below for discussion). To a good approximation $G(x,t)$ turns out to be a linear superposition of both contributions. Approximately, one gets

$$G(x,t) = [1 - f_{jump}^{1.2}(t)]G_{fluc}(x,t) + f_{jump}^{1.2}(t)\, G_{jump}(x,t) \tag{10}$$

Then $G(x,t)$ displays two different slopes from which the individual dynamic order parameters as well as the fraction $f_{jump}(t)$ can be extracted. One important aspect of the analysis is that a symmetric spectrum merely requires the final orientation of a nuclear site completely lacking correlation to the initial orientation. With all positions on a unit sphere accessible, this indeed corresponds to full isotropization expressed as $R(\beta) = \sin \beta$. In the case of geometrical restrictions, e.g. strict uniaxial rotations or exchange between a limited number of positions, the experiment is sensitive to the correlations in the accessible orientation phase space; equilibration of segments with respect to the initial orientation results in symmetric spectra, even if full isotropisation cannot be reached.

III. Experimental Section

The synthesis of amorphous PEMA selectively deuterated at the methylene and methyl moiety of the main chain is described elsewhere.[22] The sample had a weight average molecular weight of 106 000 g/mol and a polydispersity of 1.38. The tacticity was obtained by high resolution ^{13}C NMR at 125.8 MHz, yielding 62% rr (syndiotactic) triads, 35% mr triads, and 3% mm triads. The glass transition temperature measured by DSC at a heating rate of 10 K/min was 345 K.

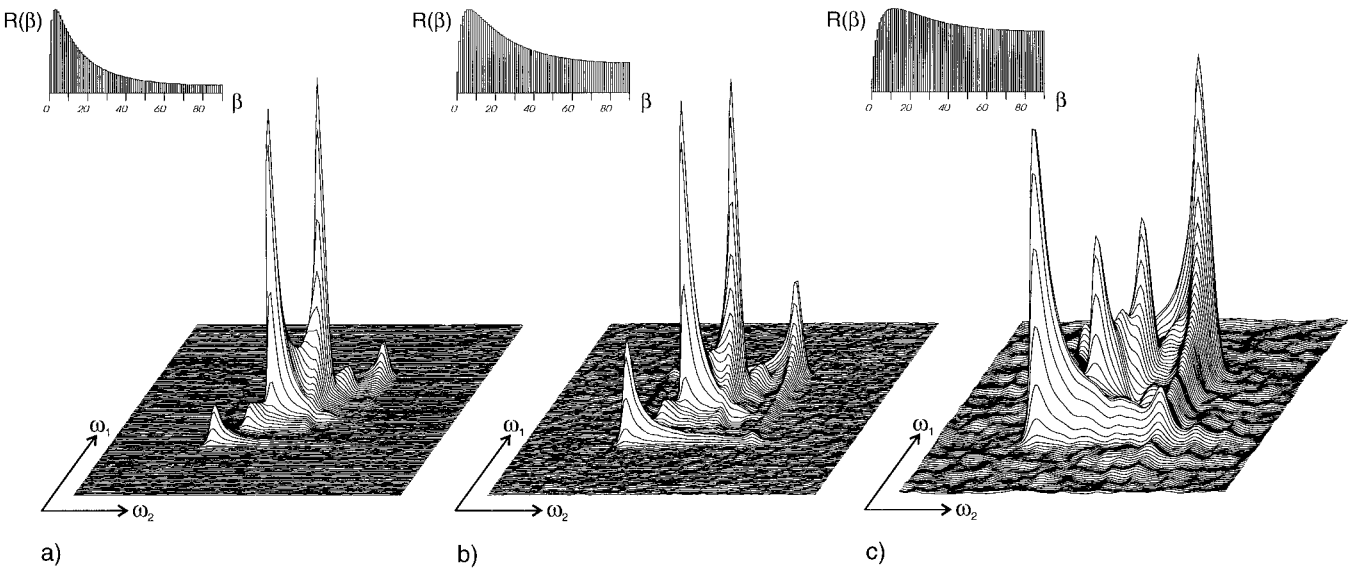

Figure 4. 2D exchange spectra of PEMA at 365 K with mixing times of (a) 5 ms, (b) 20 ms, and (c) 50 ms. The exchange intensity spread out in the whole frequency plane and the absence of characteristic ridges are typical for a broad distribution of reorientation rates and angles. The corresponding reorientation angle distributions $R(\beta)$ obtained by a simulation based on isotropic rotational diffusion with an average correlation time of 20 ms and a distribution of 2 decades (fwhm) are shown as well.

^{2}H NMR spectra were recorded on a Bruker ASX 500 spectrometer operating at a resonance frequency of 76.8 MHz with 90° pulse lengths of 2.5 μs. Generally, 256 complex data points were acquired in the detection period. For the 2D exchange spectra, the dwell time was set to 1.6 μs, corresponding to a spectral width of 312 kHz (TPPI), and for the DICO spectra, a dwell time of 1.2 μs (spectral width of 416 kHz) was used. In the indirect dimension, between 35 and 60 increments were taken with a dwell time of 3.2 μs for the 2D spectra and 2.4 μs for the DICO spectra, respectively. Further experimental details and data processing are described in the literature.[23,24]

IV. Results and Discussion

(a) 2D Exchange NMR. All multidimensional NMR spectra were recorded at 365 K, 20 K above the caloric glass transition. At this temperature, the β-process resembles its motional geometry in the glassy state, comprising a π-flip of the carboxyl group coupled to a restricted main chain rotation. It is noteworthy that, although in the molten state, the side group dynamics retains its anisotropic character.[17,18] Figure 4 shows the 2D exchange spectra of PEMA, selectively deuterated at the main chain at mixing times of 5, 20, and 50 ms, which were also chosen to be t_{ma} in the DICO spectra below. Due to the rapid rotation of the methyl group around its C_3-symmetry axis, the **EFG** tensor of the methyl deuterons is reduced by a factor of $-1/3$, giving rise to the motionally averaged Pake spectrum in the center of the 2D frequency plane. The outer singularities correspond to the signal of the methylene sites. The off-diagonal intensity of the 2D spectra is spread over the whole frequency plane and increases with longer mixing times. The absence of any characteristic exchange ridges results from a wide distribution of reorientation angles, as is found in a variety of amorphous polymers. The relative loss of total intensity of the inner subspectrum is caused by the fast spin−lattice relaxation of the methyl groups. Presented as well are the corresponding simulated RADs, where $R(\beta)$ was obtained from a fit based on the model of isotropic rotational diffusion. By comparison with a whole series of experimental spectra, the average correlation time is extracted as $\langle\tau_c\rangle = 20 \pm 5$ ms with a log-Gaussian distribution of 2 ± 0.3 decades (full width at half maximum, fwhm).

For the relatively wide distribution and small correlation time, the slow motion limit is not fully justified, especially when considering the coupling of the main chain motion to the fast side group motion. When taking into account the dynamics during the evolution and detection time in the simulations of the 2D spectra,[13,26] the average correlation time reduces to 12 ± 5 ms with a slightly higher distribution width (fwhm) of 2.4 ± 0.3 decades. The correlation time for the β-process at this temperature is less than 1 ms;[17] therefore, the 2D spectra are reflecting the α-relaxation at times longer than the main chain fluctuations combined with the carboxyl flips.

However, due to the complexity of polymer dynamics, such reorientation angle distributions may also be caused by other mechanisms, e.g. a combination of librations and a rotation around the local chain axis with varying fractions. For PEMA in particular, the anisotropy of the β-process is likely to influence the main chain dynamics on short time scales. In principle it is possible to extract the RAD directly by analyzing the intensity of the edge slice of a 2D spectrum.[27] Because of noise and excitation problems, this approach often leads to unsatisfactory results, especially when broad RADs are present. Therefore, it is desirable to get a model-free measure of the geometry of motion, in particular to separate different contributions. This approach will be presented below.

(b) Analysis of the DICO Spectra of PEMA. When recording the DICO spectra, different values for t_{mb} were chosen at fixed t_{ma} to monitor the dynamic evolution of $\langle P_2(t)\rangle$. For $t_{ma} = 20$ ms, the results are displayed in Figure 5. The contour plots are shown as insets, with linear levels taken between 1.5% and 30% of the methylene singularities to facilitate comparison. The 1D spectrum appears at the slice along the $\omega_d = 0$. For short t_{mb}, the spectra are highly asymmetric, which is visualized best at the ridges parallel to $\omega_3 = \pm\delta/2$ of the methylene tensor. With longer t_{mb}, the spectra approach their symmetric limit, almost reached at $t_{mb} = 50$ ms (cf. Figure 5d). In principle, the degree of

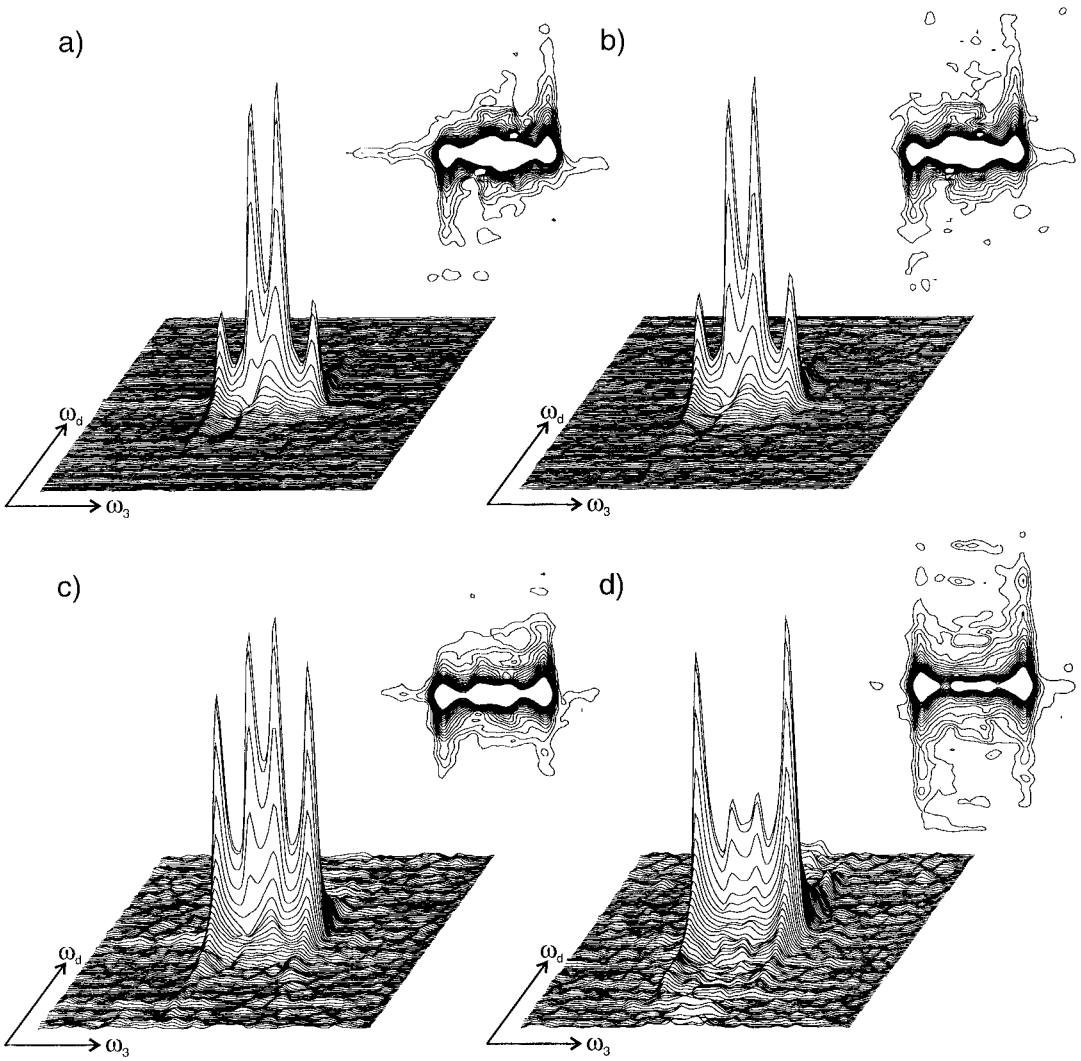

Figure 5. DICO spectra of PEMA at 365 K for $t_{ma} = 20$ ms and (a) $t_{mb} = 1$ ms, (b) $t_{mb} = 5$ ms, (c) $t_{mb} = 20$ ms and (d) $t_{mb} = 50$ ms. With increasing t_{mb}, the spectra become symmetric with respect to the slice along $\omega_d = 0$, most pronounced at the singularities of the methylene tensor of the contour plots. This is related to a decreasing dynamic order parameter approaching zero when equilibration of orientations with time is reached as is analyzed in Figure 6.

anisotropy can be obtained from any slice parallel to ω_d. Since the exchange intensity is strongest at the singularities of the 1D spectrum, i.e. $\omega_3 = \pm\delta/2$, it is advantageous to consider the ratio $G(x,t) = g(\omega_d,-\delta/2)/g(-\omega_d,-\delta/2)$ at the methylene sites. Additionally, analysis of the other slices interferes with exchange intensity caused by the methyl subspectra, that are subject to relaxation effects prohibiting a reliable analysis. The choice $\omega_3 = \pm\delta/2$ also ensures the intensity arising from the second spin transition of the ^{2}H nuclei to be small.

Figure 6 displays a semilogarithmic plot of $G(x,t)$ versus x for $t_{ma} = 20$ ms and a series of t_{mb}. Two different contributions are visible, as indicated by the straight lines serving as a guide to the eye. A discontinuity is located at $\omega_d/\delta \approx 0.25$. Clearly, small angle motions are responsible for the slope between $x = 0$ and $x = 0.25$. The smaller slope for larger x accounts for a different type of motion with larger reorientation angles; hence, the reorientation dynamics is bimodal. This directly demonstrates that a simple rotational diffusion model is not applicable, since in the case of a diffusion constant (D), only a single slope occurs that would vary like $\exp(-6Dt_{mb})$. The slower loss of orientational correlations for the second component can be explained in two ways. It can be either brought about by segments diffusing with a faster rate or by jump-type motions.

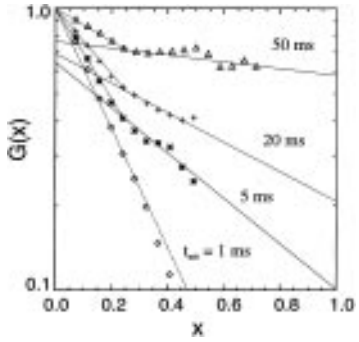

Figure 6. A plot of $G(x,t)$ versus x for $t_{ma} = 20$ ms and different t_{mb} obtained from the DICO spectra of PEMA at 365 K. The straight lines serve as guide to the eye to visualize two contributions. The different types of motion, namely fluctuations (dashed line) and large angle reorientations (solid line) can be separated and account for the discontinuity at $x \approx 0.25$. Extrapolation of the solid lines to $G(x,t) = 0$ yields the relative fraction of segments with jump-type motions. The quantitative analysis is presented in section a of Table 1.

Interestingly, the order parameter decreases only slightly between $t_{mb} = 5$ and 20 ms, whereas it has almost vanished for $t_{mb} = 50$ ms. For diffusive motion one would expect a gradual decrease of the order parameter with t_{mb}. In contrast, for jump-type motions one an-

ticipates a limiting value for small t_{mb} depending on the typical jump angle. In Figure 6, the data seem to agree better with the second possibility. It is also visible that the fraction of segments performing jumps, $f_{jump}(t)$, which can be obtained by extrapolation to $x = 0$ (see eq 10), is slowly increasing from 0.67 to 0.8, indicating that about 20% of the segments undergo only fluctuations around their initial position even for times as long as $t_{mb} = 50$ ms.

Jump-type motions are linked to conformational transitions which have been observed above the glass transition by 2D MAS exchange NMR via the γ-gauche effect.[28] In PEMA, a quantitative analysis proves to be difficult since the differences in chemical shifts for different conformations are small, resulting from a complicated dependence of the γ-gauche effect on the molecular constitution.[29]

For $t_{mb} = 1$ ms, the DICO spectrum is completely determined by small angle diffusion having a single slope. The results of the quantitative analysis of $\langle P_{2,jump}(t)\rangle$ and $f_{jump}(t)$ are given in Table 1, with errors on the order of 0.05. The analysis could not be performed for $x > 0.7$ for lack of sufficient exchange intensity and concurrent noise problems. The order parameter for fluctuations is quite high (estimated to be about 0.9) for the shortest mixing time of 1 ms and is reduced concomitant with the increasing fraction of jump-type motions for longer t_{mb} to a value of approximately 0.5. While for $t_{mb} = 5$ ms, $\langle P_{2,jump}(t)\rangle$ is as high as 0.55 with $\langle P_{2,jump}(t)\rangle = 0.13$, the correlations are almost lost for $t_{mb} = 50$ ms. Since the order parameter does not vanish for mixing times comparable to the rotational correlation time, a random jump model can also be excluded. If this were applicable, $\langle P_{2,jump}(t)\rangle$ would be equal to zero for all t_{mb} with only $f_{jump}(t)$ increasing. The results above are also corroborated by molecular dynamics simulations of a polyethylene-like chain,[30,31] where at T_g a bimodal distribution of reorientation angles was revealed, corresponding to small angle fluctuations around the equilibrium torsion angles and conformational transitions. At higher temperatures, however, the RAD could be described basically by rotational diffusion, hindered by the presence of neighboring chains.

It has been shown previously that $G(x,t)$ is largely independent of the rotational dynamics during t_{ma}.[21] This can be traced back to the fact that the dependence of the total intensity cancels by taking the ratio $G(x,t)$ and most intensity is localized around the singularities. This prediction was checked by recording DICO spectra with t_{ma} set to 5 and 50 ms.

For $t_{ma} = 5$ ms, a plot of $G(x,t)$ versus x is given in Figure 7a, and the analysis is shown in section b of Table 1. For lack of sufficient exchange intensity, $G(x,t)$ was only evaluated for $x \leq 0.6$. With short t_{mb}, the discontinuity of the slope is just perceptible, marking the onset of jump-type motions and excluding pure diffusion, as was found for $t_{ma} = 20$ ms and $t_{mb} = 1$ ms (cf. Figure 6). Though marked by the lines in the plot, the contribution of jumps and diffusion are not well separable, as is also indicated by the nearly constant value of $f_{jump}(t)$ for all mixing times. It is likely that on such a short time scale not enough jumps take place so that the decomposition of eq 9 is not justified. For $t_{mb} = 50$ ms, large angle reorientations can be distinguished. While compared to Figure 6, $f_{jump}(t)$ is of the same value, $\langle P_{2,jump}(t)\rangle$ is slightly higher for shorter mixing times t_{ma}.

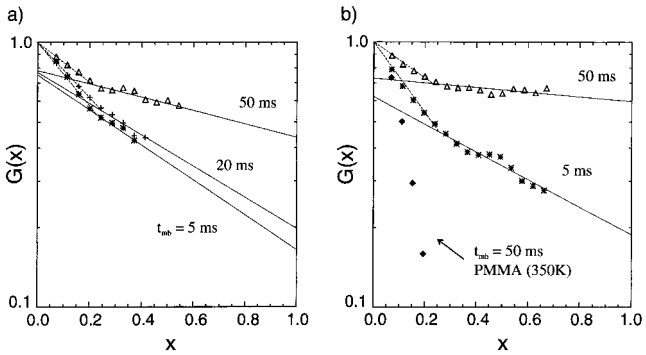

Figure 7. (a) $G(x,t)$ versus x for $t_{ma} = 5$ ms. Jumps and fluctuations are not clearly distinguishable for $t_{mb} = 5$ and 20 ms. For $t_{mb} = 50$ ms, the order parameter is slightly higher than in Figure 6. (b) $G(x,t)$ versus x for $t_{ma} = 50$ ms; for short t_{mb}, $\langle P_{2,jump}(t)\rangle$ is slightly higher. To compare the dynamics to that in the glassy state, the analysis was also performed for PMMA at 355 K with $t_{ma} = 50$ ms and $t_{mb} = 50$ ms. Below T_g, the fluctuations are smaller; see also Figure 8.

Table 1. Dynamic Order Parameters in PEMA for Jumps and Their Relative Fraction for Different t_{mb}

t_{mb} (ms)	$\langle P_{2,jump}(t)\rangle$	$f_{jump}(t)$
	(a) $t_{ma} = 20$ ms	
5	0.55	0.67
20	0.38	0.73
50	0.13	0.78
	(b) $t_{ma} = 5$ ms	
5	0.5	0.75
20	0.47	0.78
50	0.21	0.80
	(c) $t_{ma} = 50$ ms	
5	0.41	0.66
50	0.08	0.77
	(d) Average Order Parameters and Jump Fractions from Sections a−c	
5	0.49	0.69
20	0.43	0.76
50	0.14	0.79

Likewise, the analysis of DICO spectra was performed for a mixing time $t_{ma} = 50$ ms, which is longer than the average rotational correlation time. The symmetry analysis is presented in Figure 7b, and the results are given in section c of Table 1. For the second mixing time of 50 ms, the value obtained for $\langle P_{2,jump}(t)\rangle$ is about 0.1 and thus nearly the same as those of section a of Table 1. This also applies to $f_{jump}(t)$, demonstrating that for longer t_{ma} the overall fraction of molecules undergoing jumps does not increase. In contrast, the dynamic order parameter for $t_{mb} = 5$ ms is slightly smaller, indicating a faster decrease of orientational correlations. This small effect is only observable on a short time scale and is leveled out within 50 ms. Nevertheless, it seems that within the experimental errors, the dynamics is independent of t_{ma}. Taking the average values from sections a−c of Table 1, one gets approximately the results for $t_{ma} = 20$ ms; see section d of Table 1. If one incorporates the average values of section d of Table 1 in Figure 6 (not shown for clarity), slight deviations are only perceptible for $t_{mb} = 5$ ms. Thus the results of our DICO analysis are essentially independent of t_{ma}.

To give a comparison of the fluctuations solely associated with the dynamics of the β-process, below the glass transition temperature, 2D and DICO spectra of PMMA-d_5 in the glassy state at 355 K are shown in Figure 8. The mixing times were set to 50 ms, significantly longer than the correlation time of about a millisecond of the β-relaxation at that temperature. In

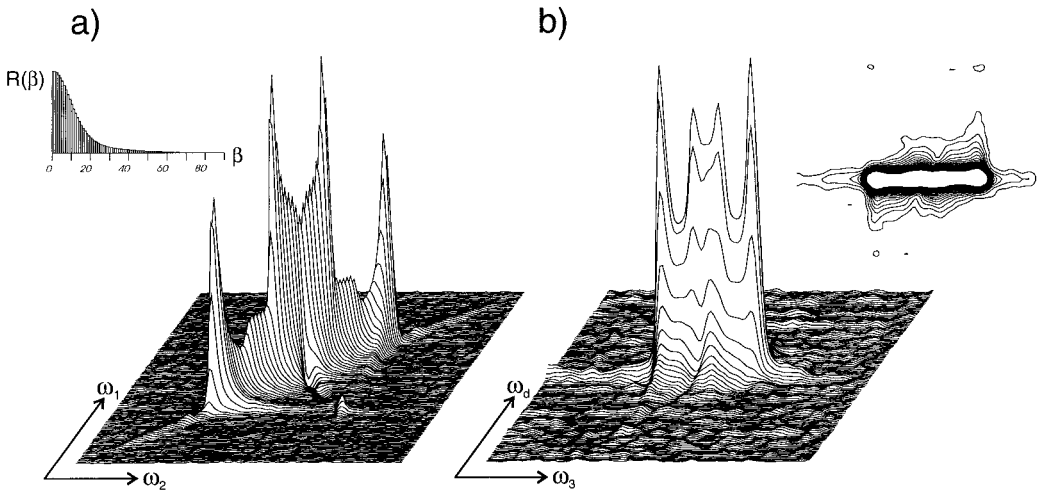

Figure 8. (a) 2D spectrum of PMMA-d_5 at 355 K (T_g − 40 K) in the glassy state with a mixing time of 50 ms. (b) corresponding DICO spectrum with $t_{ma} = t_{mb} = 50$ ms to compare the small angle fluctuations of the main chain below and above T_g as analyzed in Figure 7b.

Table 2. Dynamic Order Parameters in PS for Jumps and Their Relative Fraction for t_{ma} = 10 ms and Different t_{mb}

t_{mb} (ms)	$\langle P_{2,jump}(t)\rangle$	$f_{jump}(t)$
5	0.27	0.57
10	0.18	0.69
50	0.02	0.89

fact, those restrictions remain even for longer times and are identical to those found for PEMA below T_g.[22] The DICO spectrum is highly asymmetric, also visible in the analysis in Figure 7b, indicating nonequilibration of the segmental orientation. For a quantitative analysis, higher moments have to be incorporated, which we have not done. Obviously, the anisotropy is much higher for the fluctuations below T_g, demonstrating stronger correlations and smaller librational angles than those associated even in the limit of short t_{mb} in the molten state. This confirms earlier conclusions from of the ^{13}C 2D exchange spectra of the ester side group in PEMA.[17]

We would like to mention that the total number of segments rearranging by large angles generally does not exceed a fraction of 0.8 and, above all, is only gradually increasing with t_{mb}. Thus there is evidence for segments being trapped in their environment on a time scale of at least 50 ms. It is worth noting that in recent MD simulations on bulk PE a nonuniform distribution of conformational transitions near T_g was observed.[32] As the temperature was lowered, jumps became more localized at certain bonds. Since this behavior was not found in isolated chains, these heterogeneities were ascribed to a bulk effect of surrounding chains.

(c) Comparison with Polystyrene. With a detailed geometrical analysis of the α-relaxation available, differences for various polymers may be probed, especially the influence of the microscopic structure. Therefore, in this section, the present results will be discussed in context with those obtained previously for PS, given in Table 2.[21] The spectra of PS were recorded 13 K above the glass transition temperature with t_{ma} set to 10 ms, equal to the average rotational correlation time obtained by analyzing a series of 2D spectra at the same temperature. The results will be compared to those of PEMA with t_{ma} of 20 ms, which is approximately the average correlation time extracted from the simulations of the 2D spectra (cf. section IV.a). For large angle reorientations an average correlation time can be also estimated from the DICO spectra by the condition $1 - f_{jump}(t) = 1/e$; however, this measure is not very accurate. Since in PEMA the fraction of segments undergoing large angle motions increases only gradually, the average correlation time is estimated to be between 5 and 20 ms, consistent with the analysis of the 2D spectra.

Clearly, if one compares the data with similar values of $f_{jump}(t)$, like $t_{mb} = 5$ or 20 ms for PEMA and $t_{mb} = 10$ ms for PS, the order parameter for jump-type motions is significantly higher in PEMA. At a time about twice as large as $\langle\tau_c\rangle$, the order parameter in PEMA is still almost as high as in PS. Hence, the orientations accessible by a typical jump are more restricted in PEMA. The effective jump angles are smaller, accounting for a lower equilibration of orientations. This demonstrates that there exists a preference to reorient along a specific direction, consistent with the earlier conclusion from ^{13}C NMR[17] that the π-flip of the carboxyl group of the β-process is associated with a uniaxial local rotation perpendicular to the chain axis. Due to conformational transitions,[29] this local chain direction is eventually lost on a longer time scale on which the dynamics leads to an isotropic distribution. Already for short mixing times t_{mb}, $f_{jump}(t)$ is rather high in PEMA. The increase with t_{mb} is distinctly slower. In other words, a higher fraction of segments stays trapped in its local environment, performing only small angle fluctuations, which are an essential feature of the dynamics in poly(methacrylates).

V. Summary

By applying 3D difference correlated spectroscopy, previously inaccessible details about the geometry of the dynamics in PEMA have been elucidated without employing a specific model. The bimodal nature of the geometry of reorientation dynamics in amorphous polymers was corroborated by separating small angle fluctuations from large angle motions and determining their relative importance. The dependence of molecular orientations with time were analyzed quantitatively in terms of a dynamic order parameter, $\langle P_2(t)\rangle$, as a transient measure of orientational correlation. Generally, several jump-type processes are necessary to achieve equilibration of orientations of molecular segments; thus, single motional processes are not random in nature. At this point it is not clear whether this mainly reflects restrictions of the segmental motion due

to the connectivity within the macromolecule or is due to interchain packing effects. The comparison of the dynamics in PEMA and PS reveals effective jump angles to be smaller in the former. Further information about the restriction of chain motion is provided by the fraction of jump-type motions. Approximately 20% of the groups remain trapped in their environment in PEMA, whereas essentially all groups reorient in PS on the same relative time scale. Additionally, small angle diffusion, coupled to the β-relaxation, is more pronounced in PEMA, indicated by the nonseparable contribution of jumps and librations on a short time scale. Thus, by comparing the dynamic order parameter of different glass-forming materials, many subtle features due to microscopic structure and packing should be accessible in the future.

Acknowledgment. We thank U. Pawelzik for synthesizing the labeled samples and Dr. J. Leisen for valuable discussions. Financial support from the Deutsche Forschungsgemeinschaft (SFB 262) is gratefully acknowledged.

References and Notes

(1) McCrum, N. G.; Read, B. E.; Williams, G. *Inelastic and Dielectric Effects in Polymeric Solids*; Wiley, New York, 1991.
(2) Ferry, J. D. *Viscoelastic Properties of Polymers*; 3rd ed.; Wiley: New York, 1980.
(3) Richert, R.; Blumen, A. *Disorder Effects on Relaxational Processes*, Springer Verlag, Berlin, 1994.
(4) Monnerie, L. *Makromol Chem. Macromol. Symp.* **1991**, *48*/*49*, 125.
(5) Garwe, F.; Schönhals, A.; Lockwenz, H.; Beiner, M.; Schröter, K.; Donth, E. *Macromolecules* **1996**, *29*, 247−253.
(6) Patterson, G. D.; Stevens, J. R.; Lindsey, B. P. *J. Macromol. Sci., Phys.* **1980**, *18*, 641.
(7) Fytas, G.; Patkowski, A.; Meier, G.; Dorfmüller, Th. *Polymer* **1983**, *24*, 2214.
(8) Schmidt-Rohr, K.; Spiess, H. W. *Multidimensional Solid State NMR and Polymers*; Academic Press: New York, 1994.
(9) Schmidt, C.; Wefing, S.; Blümich, B.; Spiess, H. W. *Chem. Phys. Lett.* **1986**, *130*, 84.
(10) Wefing, S.; Kaufmann, S.; Spiess, H. W. *J. Chem. Phys.* **1988**, *89*, 1234.
(11) Pschorn, U.; Rössler, E.; Sillescu, H.; Kaufmann, S.; Schaefer, D.; Spiess, H. W.; *Macromolecules* **1991**, *24*, 398.
(12) Schaefer, D.; Spiess, H. W.; Suter, U. W.; Fleming, W. W. *Macromolecules* **1990**, *23*, 3431.
(13) Schaefer, D.; Spiess, H. W. *J. Chem. Phys.* **1992**, *97*, 7944.
(14) Schmidt-Rohr, K.; Spiess, H. W. *Phys. Rev. Lett.* **1991**, *66*, 3020.
(15) Leisen, J.; Schmidt-Rohr, K.; Spiess, H. W. *J. Non-Cryst. Solids* **1994**, *172*−*174*, 737.
(16) Schmidt-Rohr, K.; Kulik, A. S.; Beckham, H. W.; Ohlemacher, A.; Pawelzik, U.; Boeffel, C.; Spiess, H. W. *Macromolecules* **1994**, *27*, 4733.
(17) Kulik, A. S.; Beckham, H. W.; Schmidt-Rohr, K.; Radloff, D.; Pawelzik, U.; Boeffel, C.; Spiess, H. W. *Macromolecules* **1994**, *27*, 4746.
(18) Kulik, A. S.; Radloff, D.; Spiess, H. W. *Macromolecules* **1994**, *27*, 3111.
(19) Fytas, G.; Meier, G.; Dorfmüller, Th.; Patkowski, A. *Macromolecules* **1982**, *15*, 214.
(20) Domberger, W.; Reichert, D.; Garwe, F.; Schneider, H.; Donth, E. *J. Phys.: Condens. Matter* **1995**, *38*, 7419.
(21) Heuer, A.; Leisen, J.; Kuebler, S. C.; Spiess, H. W. *J. Chem. Phys.*, in press.
(22) Kuebler, S. C.; Boeffel, C.; Pawelzik, U.; Spiess, H. W., to be published.
(23) Schmidt, C.; Blümich, B.; Spiess, H. W. *J. Magn. Res.* **1988**, *79*, 390.
(24) Schaefer, D.; Leisen, J.; Spiess, H. W. *J. Magn. Res. A* **1995**, *115*, 60.
(25) Spiess, H. W. In *Developments in Oriented Polymers*; Ward, I. M., Ed.; Applied Science Publishers: Oxford, UK, 1982; Vol. 1, Chapter 2.
(26) Kaufmann, S.; Wefing, S.; Schaefer, D.; Spiess, H. W. *J. Chem. Phys* **1990**, *93*, 197.
(27) Hagemeyer, A.; Brombacher, L.; Schmidt-Rohr, K.; Spiess, H. W. *Chem. Phys. Lett.* **1990**, *167*, 583.
(28) Zemke, K.; Chmelka, B. F.; Schmidt-Rohr, K.; Spiess, H. W. *Macromolecules* **1991**, *24*, 6874.
(29) Zemke, K., PhD thesis, Mainz, 1994.
(30) Takeuchi, H.; Roe, R.-J. *J. Chem. Phys.* **1991**, *94*, 7446.
(31) Takeuchi, H.; Roe, R.-J. *J. Chem. Phys.* **1991**, *94*, 7458.
(32) Boyd, R. H.; Gee, R. H.; Han, J.; Jin, Y. *J. Chem. Phys.* **1994**, *101*, 788.

MA960911M